Title: Inhibitory interneurons show early dysfunction in a SOD1 mouse model of Amyotrophic Lateral Sclerosis

Running Title: Dysfunction of inhibitory interneurons in ALS

C. F. CAVARSAN[1,2], P. R. STEELE[1,2,3], L. M. McCANE[3], K. J. LaPRE[1,2], A. C. PURITZ[4], N. KATENKA[5], AND K. A. QUINLAN[1,2,4]

1 George and Anne Ryan Institute for Neuroscience, University of Rhode Island, Kingston, RI, 02881 USA

2 Department of Biomedical and Pharmaceutical Sciences, College of Pharmacy, University of Rhode Island, Kingston, RI, 02881 USA

3 Interdisciplinary Neuroscience Program, University of Rhode Island, Kingston, RI, 02881 USA

4 Department of Physiology, Northwestern University Feinberg School of Medicine, Chicago, IL, 60611 USA

5 Department of Computer Science and Statistics, University of Rhode Island, Kingston, RI, 02881 USA

Corresponding Author:

Katharina A. Quinlan (https://orcid.org/0000-0002-6177-4849)

kaquinlan@uri.edu

George and Anne Ryan Institute for Neuroscience

University of Rhode Island

130 Flagg Rd

Kingston RI 02881

Category according to the table of contents: Neuroscience

Key words: inhibition, glycine, Renshaw cells, amyotrophic lateral sclerosis, spinal cord, patch clamp.

Key Points Summary:

- Spinal inhibitory interneurons could contribute to amyotrophic lateral sclerosis (ALS) pathology, but their excitability has never been directly measured.
- We studied the excitability and morphology of glycinergic interneurons in postnatal transgenic mice ($SOD1^{G93A}$GlyT2eGFP).
- Interneurons were less excitable and had smaller somas but larger primary dendrites in SOD1 mice.
- GlyT2 interneurons were analyzed according to their localization within the ventral spinal cord. Interestingly, the greatest differences were observed in the most ventrally-located interneurons.
- We conclude that inhibitory interneurons show presymptomatic changes that may contribute to excitatory / inhibitory imbalance in ALS.

Abstract: Few studies in amyotrophic lateral sclerosis (ALS) focus on the inhibitory interneurons synapsing onto motoneurons (MNs). However, inhibitory interneurons could contribute to dysfunction, particularly if altered before MN neuropathology and establish a long-term imbalance of inhibition / excitation. We directly assessed excitability and morphology of glycinergic (GlyT2) interneurons located throughout the ventral horn in the lumbar enlargement from $SOD1^{G93A}$GlyT2eGFP (SOD1) and wildtype GlyT2eGFP (WT) mice on postnatal day 6 to 10. Patch clamp revealed dampened excitability in SOD1 interneurons, including depolarized persistent inward currents (PICs), depolarized threshold for firing action potentials, and a shortened afterhyperpolarization (AHP). SOD1 inhibitory interneurons also had smaller somata but primary dendrites showed larger volume and surface area than WT. GlyT2 interneurons were then divided into 3 subgroups based on location: (1) interneurons within 100 µm of the ventral white matter, where Renshaw cells (RCs) are located, (2) interneurons interspersed with MNs in lamina IX, and (3) interneurons in the intermediate ventral area including laminae VII and VIII. Ventral interneurons were the most profoundly affected, including more depolarized PICs, smaller somata and larger primary dendrites. Interneurons in lamina IX had depolarized PIC onset, smaller somata and longer primary dendrites. In lamina VII-VIII, interneurons were largely unaffected, mainly showing smaller somata. In summary, inhibitory interneurons show very early region-specific perturbations poised to impact excitatory / inhibitory balance of MNs, modify motor output, and provide early biomarkers of ALS. Therapeutics like riluzole which universally reduce CNS excitability could exacerbate the inhibitory dysfunction described here.

Abstract Figure:

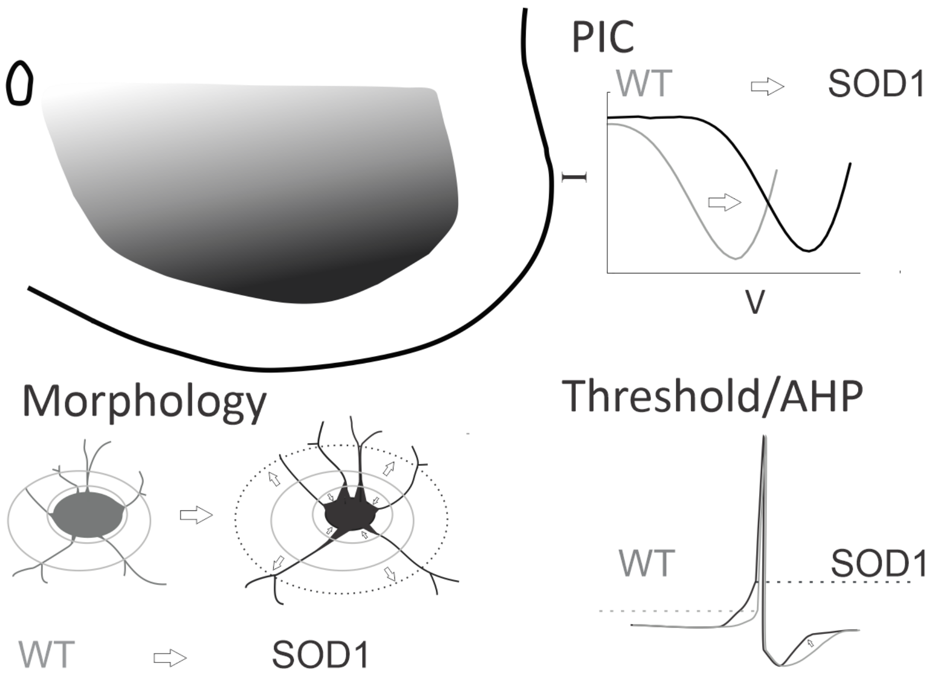

Abstract Figure: SOD1 glycinergic interneurons in the ventral horn show altered morphology and excitability, including depolarization of PICs, depolarized threshold, shorter AHPs, smaller somata and larger primary dendrites. Ventrally located interneurons are the most prominently affected.

Introduction

Amyotrophic lateral sclerosis (ALS) is a rapidly evolving adult-onset neurological disease characterized by a progressive loss of corticospinal neurons and MNs. There has been considerable debate in the field over the role of hyperexcitability in neurodegenerative processes in ALS. While drug treatment for ALS based on nonspecific reduction of neuronal excitability (with riluzole, for example) (Bellingham 2011), results in a modest increase in lifespan (Bensimon et al., 1994), similar treatment paradigms have been disappointing clinically. A more nuanced understanding of the excitability of vulnerable neurons could help in creating a more targeted and effective approach for treatment of ALS. For example, if inhibitory pathways are failing in ALS and neuronal excitability is universally reduced with riluzole, this could further exacerbate inhibitory dysfunction by reducing activity not only in vulnerable MNs but also in inhibitory interneurons presynaptic to MNs. Thus it is important to consider all aspects of neuronal excitability, including intrinsic excitability of vulnerable neurons, synaptic drive, and neuromodulation (Gunes et al., 2020). Intrinsic properties of MNs have been well studied but the same is not true for interneurons that are synaptically connected to them. In fact, no studies thus far have directly assessed activity of spinal premotor interneurons in an ALS model.

Despite evidence that ALS patients have disrupted inhibition at spinal levels (Raynor and Shefner, 1994; Shefner and Logigian, 1998; Sangari et al., 2016; Howells et al., 2020; Özyurt et al., 2020), much is still unknown concerning the involvement of inhibitory circuitry in ALS. Morphological alterations in inhibitory circuits have been demonstrated in animal models of ALS. These include degeneration of spinal interneurons, fewer neurons expressing markers of inhibitory neurotransmitters including GlyT2 prior to loss of MNs (Martin et al., 2007; Hossaini et al., 2011), and loss of glycinergic boutons onto MNs prior to symptom onset (Chang and Martin, 2009a). Typically, fast MNs have greater numbers of inhibitory synaptic contacts, but these are largely lost in SOD1 mice beginning when motor unit atrophy is first observed (Pun et al., 2006; Hegedus et al., 2007; Allodi et al., 2021). Recurrent inhibitory circuits mediated by RCs are impaired before symptom onset by both loss of MN collaterals which provide synaptic drive, and complex changes to RC-MN synaptic structures (Casas et al., 2013; Wootz et al., 2013). A few studies have suggested activity is decreased in inhibitory interneurons by indirect measurements. Quantification of synaptic inputs to MNs has shown that frequency of inhibitory postsynaptic potentials in spinal MNs is decreased embryonically in both SOD1 mouse and zebrafish models (McGown et al., 2013; Branchereau et al., 2019) and glycinergic inputs to MNs decay faster in

SOD1 MNs (Medelin et al., 2016). On a larger scale, blocking the activity of V1 inhibitory interneurons during *in vivo* treadmill running was recently found to mimic the early locomotor deficits in SOD1 mice (Allodi et al., 2021), suggesting that inhibitory interneurons could be inactive or under-active. However, none of these studies directly examined electrophysiological activity in inhibitory interneurons.

We hypothesized that inhibitory spinal interneurons could contribute to the pathogenesis of ALS through a depression of MN inhibition. Decreased activity of inhibitory interneurons could result in synaptically-driven hyperexcitability of MNs and other long-term changes in network function. In this study, we examined electrical and morphological properties of glycinergic interneurons in the spinal cord of SOD^{G93A} GlyT2-eGFP (SOD1) mice compared to GlyT2-eGFP (WT) using whole cell patch clamp and three-dimensional reconstructions. We show here that significant dysfunction is present in SOD1 glycinergic interneurons which likely comprise several subclasses of inhibitory interneurons. In general, SOD1 glycinergic interneurons are less excitable and smaller than WT. Impairment in glycinergic interneurons should be explored as both a mechanism of vulnerability of MNs and a potential biomarker of early dysfunction of spinal circuits.

Materials and Methods

Ethics Statement

Experiments were performed in accordance with the United States National Institutes of Health Guide for Care and Use of Laboratory Animals. Approval from Northwestern University's Animal Care and Use Committee (IS00001228) was obtained for all experiments performed in this study. All efforts were made to minimize animal suffering and to reduce the number of animals used.

Animals and Tissue harvest

Transgenic B6SJL mice overexpressing the human $SOD1^{G93A}$ gene (strain 002726, Jackson Labs, Bar Harbor, ME, USA) and their wild type littermates were used (nontransgenic for the human $SOD1^{G93A}$ gene). Transgenic animals were identified using standard PCR techniques by Transnetyx (Cordova, TN, USA) and were bred with GlyT2-eGFP mice (Zeilhofer et al., 2005) generating $SOD1^{G93A}$ GlyT2-eGFP mice, here called SOD1. Inhibitory glycinergic interneurons express the Na^+ and Cl^- coupled glycine transporter 2, or GlyT2 and GlyT2-eGFP expression is driven by the GlyT2 promotor. Specifically, GlyT2-eGFP females were bred with $SOD1^{G93A}$ GlyT2-eGFP males, and progeny were used for experiments before genotyping was performed. GlyT2-eGFP are referred to as wild type (WT), not carrying the $SOD1^{G93A}$ mutation. For the following studies juvenile mouse pups were used between postnatal day (P) 6 - 10. Mice were deeply anesthetized with isoflurane (Henry Schein Animal Health, Dublin, OH, USA), decapitated and eviscerated. The lumbar spinal cord from L1 - L6 was removed and embedded in 2.5% w/v agar (No. A-7002, Sigma-Aldrich, St Louis, MO, USA). The agar block was then superglued with Loctite 401 (Henkel Corporation, Rocky Hill, CN, USA) to a stainless steel slicing chuck and 350 µm transverse slices were made using the Leica 1000 vibratome (Leica Microsystems, Buffalo Grove, IL, USA) as described previously (Quinlan et al., 2011). During both spinal cord isolation and slicing, the spinal cord was immersed in 1–4°C high osmolarity dissecting solution containing (mM): sucrose 234.0, KCl 2.5, $CaCl_2 \cdot 2H_2O$ 0.1, $MgSO_4 \cdot 7H_2O$ 4.0, HEPES 15.0, glucose 11.0, and Na_2PO_4 1.0. The pH was adjusted to 7.35 when bubbled with 95% O_2/5% CO_2 using 1 M KOH (Fluka Analytical, Sigma-Aldrich). After cutting, the slices were incubated for >1 h at 30°C in incubating solution containing (mM): NaCl 126.0, KCl 2.5, $CaCl_2 \cdot 2H_2O$ 2.0, $MgCl_2 \cdot 6H_2O$ 2.0, $NaHCO_3$ 26.0, glucose 10.0, pH 7.4 when bubbled with 95% O_2/5% CO_2 (all reagents for solutions were purchased from Sigma-Aldrich).

Electrophysiology

Whole cell patch clamp was performed on interneurons from the lumbar segments using 2–4 MΩ glass electrodes pulled from glass capillary tubes (Item #TW150F-4, World Precision Instruments, Sarasota, FL, USA) with a Flaming-Brown P-97 (Sutter Instrument Company, Novato, CA, USA). Electrodes were positioned using a Sutter Instrument MP-285 motorized micromanipulator (Sutter Instrument Company). Whole-cell patch clamp measurements were performed at room temperature using the Multiclamp700B amplifier (Molecular Devices, Burlingame, CA, USA) and Winfluor software (University of Strathclyde, Glasgow, Scotland). Briefly, slices were perfused with a modified Ringer's solution containing (in mM): 111 NaCl, 3.09 KCl, 25.0 $NaHCO_3$, 1.10 KH_2PO_4, 1.26 $MgSO_4$, 2.52 $CaCl_2$, and 11.1 glucose. The solution was oxygenated with 95% O_2/5% CO_2, and the perfusion rate was 2.5 – 3.0 ml/min. Patch electrodes contained (in mM) 138 K-gluconate, 10 HEPES, 5 ATP-Mg, 0.3 GTP-Li and Texas Red dextran (150 µM, 3000 MW, from Invitrogen, Life Technologies, Grand Island, NY, USA). In voltage-clamp mode, fast and slow capacitance transients, as well as whole-cell capacitance, were compensated using the automatic capacitance compensation on the Multiclamp. Whole cell capacitance was recorded from the Multiclamp.

Neuron Selection: Glycinergic interneurons were visually selected for recording based on 1) expression of GFP, and 2) location in the ventral horn. Neurons that did not repetitively fire or did not maintain a resting membrane potential below -35 mV were excluded from electrophysiological analysis.

Electrophysiological analysis: Holding potential was set at −90 mV, and neurons were subjected to slow, depolarizing voltage ramps of 22.5 mV s^{-1}, bringing the cell to 0 mV in 4 s, and then back to the holding potential in the following 4 s. In current clamp, neurons were subjected to depolarizing current ramps for testing I-on (the current level at firing onset), I-off (the current level at cessation of firing), and the slope of the frequency–current relationship. The difference between I-on and I-off is calculated for ΔI. Negative current was often necessary to prevent action potential (AP) firing. Resting membrane potential was recorded as the potential when 0 current was injected in voltage clamp. Persistent inward current (PIC) parameters were measured after subtraction of leak current. Onset was defined as the voltage at which the current began to deviate from the horizontal, leak-subtracted trace. PIC peak was the voltage at which the PIC reached peak amplitude. The linear portion of leak current (usually between -90 and -75 mV) was used to calculate whole cell input resistance. The first action potential in the train evoked by a depolarizing current ramp in current clamp mode was used to measure all parameters relating to action potentials. Threshold voltage was defined as the voltage at which the slope exceeded 10 V/s. Threshold for action potential firing was tested in two ways. The first was to use the voltage at firing onset from the current ramps up to 130 pA/s (in current clamp). The second was the voltage at which a single action potential could be evoked with a current step. Action potential overshoot is the voltage past 0 mV the first spike (from a ramp) reaches. Duration of the action potential is measured at half of action potential height (height is defined as overshoot – threshold voltage). Rates of rise and fall are defined as the peak and the trough of the first derivative of the action potential profile. Instantaneous firing frequency range max was the maximum firing rate that could be evoked from a neuron. It was measured from the first or second firing frequencies on a large (>150pA) depolarizing step. Steady state firing frequency range minimum was the lowest firing frequency evoked from a small (~50pA) depolarizing step. Hyperpolarizing steps were used to measure I_H. The sag and rebound were measured from largest evoked response. Sag potential was calculated as a % of the total amplitude of the hyperpolarization. If a spike was evoked on rebound, the voltage threshold was used as amplitude of rebound. AHP duration was measured from a single spike fired during a period in which the membrane potential was stable. Amplitude was measured as the downward deflection from the membrane potential. Duration of the AHP was measured from the falling phase of the spike at baseline potential to the time of recovery to baseline membrane potential. Half amplitude duration was measured as the duration at half of the measured AHP amplitude from the falling phase of the spike at baseline potential. Tau is measured as the rate of decay from the last third of the AHP.

Regional classification: Photos were taken of position of the patch electrode within the spinal cord slices after recording was complete. These photos were used to recreate a map of the position of the interneurons. Interneurons within the ventral-most region of the spinal cord (within 100µm of the ventral white matter) were grouped into the RC region described previously (Siembab et al., 2010). Neurons that were located within and on the lateral edges of the motor pools (in between motoneuron and the white matter) were classified as lamina IX interneurons. Since the location of the motor pools varied throughout the lumbar enlargement, this classification was determined by examination of the z stacks and photos. Neurons that were not found within lamina IX and were not within the ventral RC region were grouped as the intermediate region of Lamina VII/VIII. All patched neurons were filled with Texas Red dextran to allow their 3D reconstruction. Reconstructions were limited to the first dendritic node (more details in following section).

Morphological analysis

Neuron morphology was assessed from two types of images: 1) 2-photon image stacks of live neurons taken immediately after obtaining electrophysiological parameters, and 2) confocal image stacks taken after fixation and tissue processing. Images collected using these two methods were analyzed separately due to tissue shrinkage during the fixation process. Measurements from patched neurons included both soma and dendrites (soma volume, soma surface area; and average [per dendrite] dendrite length, total dendrite length [per cell], average and total dendrite surface area and average and total dendrite volume). Dendrite reconstructions were performed up to the first node for several reasons, including variable dye filling of fine processes of distal dendrites and potential extension of dendrites outside of the areas imaged. Measurements of GFP+ glycinergic interneurons from fixed tissue samples included soma volume and soma surface area. Reconstructions were made based on the sum of many z stacks, resulting in 3D images. Data is generated using Neurolucida software (MBF Bioscience, Williston, VT, USA): volume is computed by sum of each section area, multiplied by the thickness; surface area is the sum of each section perimeter of the reconstruction multiplied by the thickness; dendrites are modeled as the somata but using each piece of each branch as a frustum.

Two-photon imaging: An Olympus BX-51WIF microscope fitted with an Olympus 40x/0.8NA water-dipping objective lens was used. Two-photon excitation fluorescence microscopy was performed with a galvanometer-based Coherent Chameleon Ultra II laser (Coherent, Santa Clara, CA, USA) tuned to 900 nm. A red Bio-Rad 2100MPD photomultiplier tube (Bio-Rad, Hercules, CA, USA) (570 – 650 nm) was used to collect emission in the red channel. Z-stacks were obtained for each interneuron at 1024 x 1024 pixels (308 x 308 µm) resolution and roughly 100 µm in depth (step size 1 µm). From these Z-stacks, Texas Red® -filled neurons were three-dimensionally reconstructed, as described above, using Neurolucida software.

Confocal imaging: Sections were observed with a confocal laser microscope (LSM510, Zeiss, Oberkochen, Darmstadt, Germany) with argon (488 nm) and a 20X objective. From these Z-stacks, GlyT2 positive interneurons were three-dimensionally reconstructed using Neurolucida software as described above. Dimensions of neurons in each image stack were averaged before compiling numbers. The total number of analyzed interneurons was 4,138, composed of 2,551 neurons from 36 WT image stacks and 1,587 interneurons from 44 SOD1 image stacks.

Statistical analysis

The assumptions of homogeneity of variances and the normality of the distribution of values for each measured characteristic were evaluated with Levine's and Shapiro-Wilk tests, respectively. Group comparisons (WT vs SOD1) were performed using one-way ANOVA on parameters that satisfied both conditions (homogeneity and normality of distribution) and using the Kruskal-Wallis test for those that did not. Results are presented as means +/-SEM. Significance level was set at $p \leq 0.05$.

Results

Morphology of glycinergic interneurons

Ventrally located glycinergic interneurons in the lumbar enlargement of WT and SOD1 mice postnatal day (P) 6-10 were reconstructed from z-stack images obtained using confocal microscopy. SOD1 GlyT2 interneurons were significantly smaller than WT GlyT2 interneurons. Soma volume and surface area were both significantly smaller in SOD1 GlyT2 interneurons found throughout the ventral horn. Typical ventrolateral glycinergic neurons are shown in **Figure 1**. Complete reconstructions of soma morphology were performed on 4138 GlyT2 interneurons (2551 WT and 1587 SOD1 interneurons) from fixed lumbar spinal cords from 18 mice (9 WT and 9 SOD1). See **Table 1** for all morphological parameters. Dendritic morphology was not possible in these images due to the high number of GFP+ neurons and processes but was performed on a smaller subset of neurons that were imaged live after patch clamp electrophysiology with a 2-photon microscope.

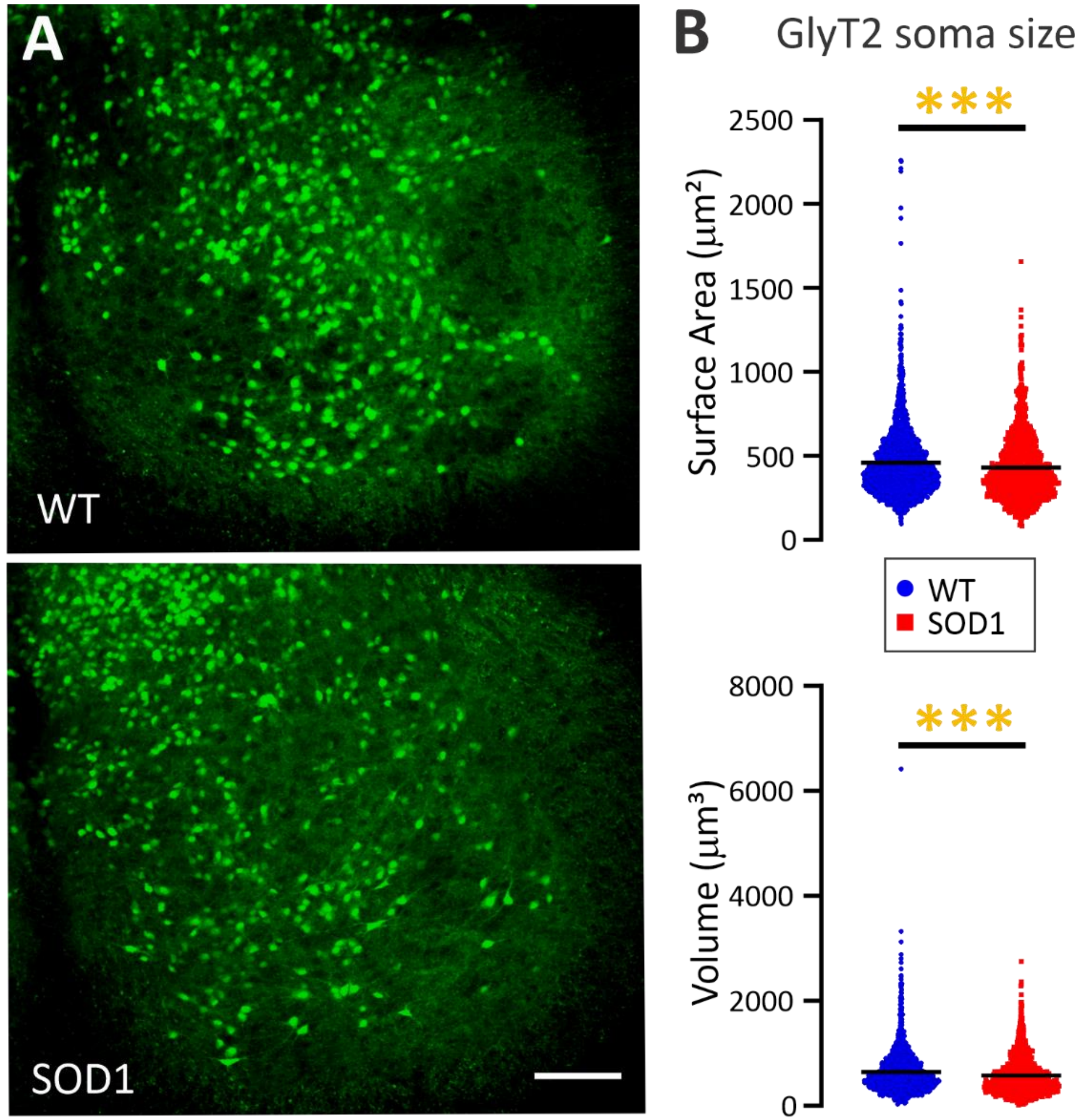

Figure 1: GlyT2 interneurons in the ventral horn from SOD1 mice are smaller than WT. Representative photomicrographs of spinal cord showing GFP interneurons (green) in **A**. (**B**) Morphological analysis showed SOD1 glycinergic interneurons in ventral horn (N = 1587) were smaller in than WT (N = 2551). Significance denoted with *** indicates $p \leq 0.001$. Scale bar in **A**: 100 μm applies to both images.

Table 1: Reconstruction data of GlyT2-GFP+ interneurons in WT and SOD1 animals.

		Ventral horn GlyT2-GFP+ Interneurons (somata only)		
		WT (Mean ± SE)	**SOD (Mean ± SE)**	***p***
		N = 2551	N = 1587	
Soma	Surface Area (µm²)	459.8 (± 4.1)	430.5 (± 4.9) ***	0.000 [K]
	Volume (µm³)	641.1 (± 8.0)	576.5 (± 9.2) ***	0.000 [K]
		Patched GlyT2-GFP+ Interneurons		
		N = 34	N =25	
Soma	Surface Area (µm²)	621.1 (± 41.6)	674.6 (± 54.8)	0.728 [K]
	Volume (µm³)	1460.2 (± 185.6)	1751.2 (± 222.6)	0.414 [K]
Primary Dendrites	Total Length (µm)	108.5 (± 21.7)	114.4 (± 10.5)	0.152 [K]
	Total Dendrite Length (µm)	101.4 (± 17.3)	103.8 (± 10.1)	0.905
	Average Dendrite length (µm)	29.3 (± 3.5)	31.3 (± 2.7)	0.663
	Total Surface Area (µm²)	539.9 (± 87.6)	700.3 (± 53.5) *	0.032 [K]
	Average Surface Area (µm²)	155.5 (± 17.5)	207.8 (± 17.9) *	0.025 [K]
	Total Volume (µm³)	272.2 (± 48.6)	423.1 (± 40.1) *	0.009 [K]
	Average Volume (µm³)	78.6 (± 11.0)	126.5 (± 13.5) *	0.008 [K]

Significance denoted with * indicates $p \leq 0.05$; *** indicates $p < 0.001$.
N is the number of cells included in analysis.
[K] Indicates Kruskal-Wallis Test for nonparametric distributions; all others were ANOVA analysis.

To study electrophysiological properties of GlyT2 interneurons, 59 glycinergic neurons (34 WT and 25 SOD1) were recorded using visually guided patch clamp with Texas Red dye in the electrode as shown in **Figure 2.** The location of patched neurons was distributed throughout the ventral horn as shown in Fig 2B. In this smaller sample of neurons, soma sizes of patched SOD1 interneurons were not different (Fig 2C). However, dendrites, analyzed up to the first node (branching point), were larger in patched SOD1 GlyT2 interneurons, including greater dendritic surface area and volume (see Table 1 for complete results). The number of primary dendrites was not different in SOD1 vs WT interneurons. Please note that dimensions of these neurons cannot be directly compared to the previous section since these neurons were imaged in living tissue while the previous analysis was performed in fixed tissue, which shrinks.

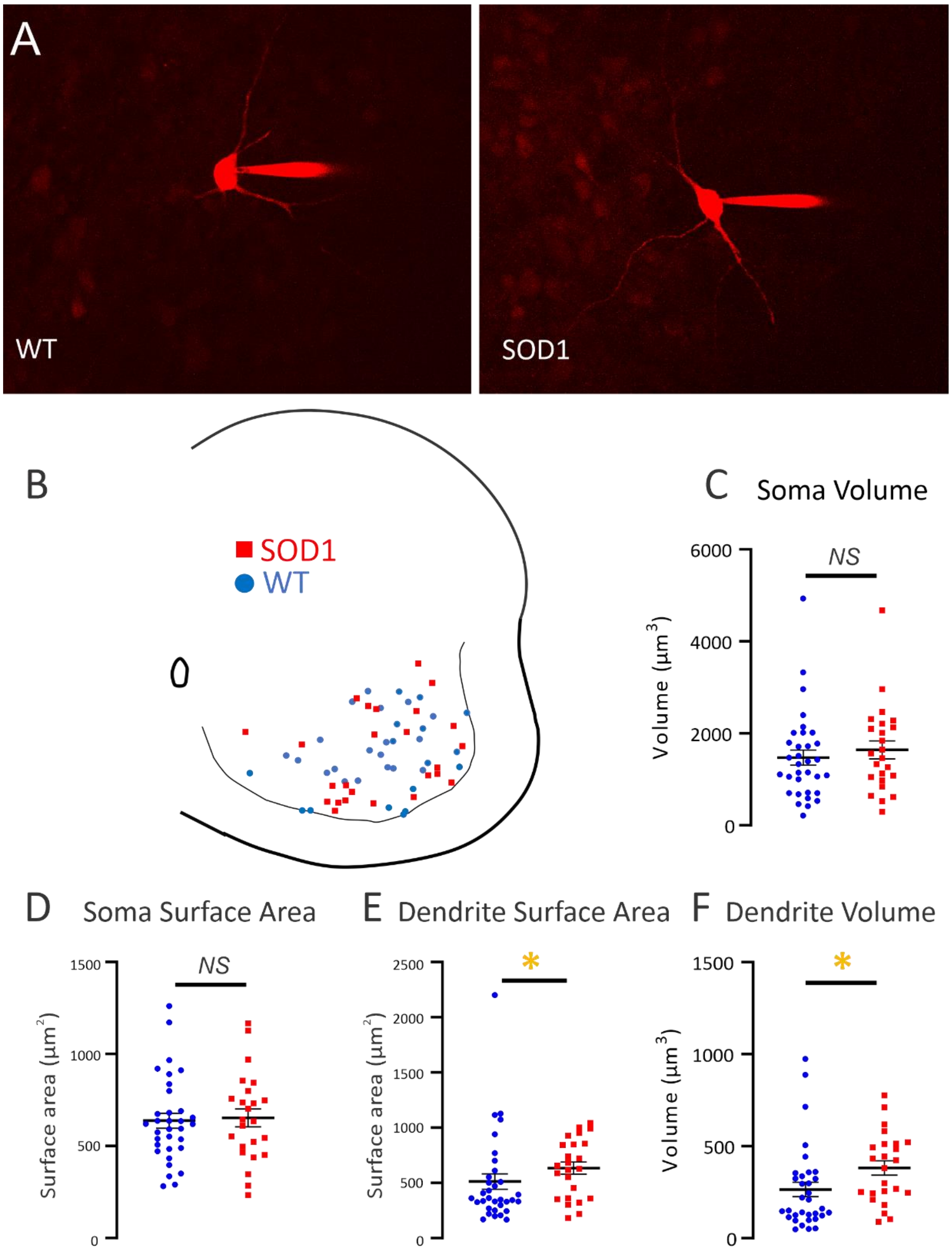

Figure 2 GlyT2 interneurons from WT and SOD1 mice were patched throughout the ventral horn. Images of typical interneurons, filled with Texas Red as they were recorded in **A**, and locations of all patched interneurons in **B** (WT = blue circles, SOD1 = red squares). (**C**) Soma volume and (**D**) soma surface area was unchanged in patched neurons, while total surface area and total volume of primary dendrites (**E** and **F**) were larger in SOD1 interneurons than in WT. Significance denoted with * indicates $p \leq 0.05$.

Electrophysiology of glycinergic interneurons

Whole cell patch clamp revealed very different intrinsic properties of ventral glycinergic interneurons. Recording was performed on 59 ventral interneurons from throughout the ventral horn in transverse lumbar spinal cord slices from P6-10 mice. SOD1 inhibitory interneurons (n = 25) were found to have diminished intrinsic excitability compared to WT interneurons (n = 34). Measurements of intrinsic excitability included depolarized onset and peak voltage of PICs and depolarized threshold for action potential firing, as shown in **Figure 3**. In voltage clamp, slowly depolarizing voltage ramps were used to measure PICs (typical leak subtracted traces shown in Fig3A). Voltage sensitivity is determined by measuring voltage at PIC onset and peak. Both PIC onset and peak were significantly depolarized in SOD1 interneurons, while amplitude of the PIC was unchanged. Depolarizing current ramps were used to measure the input-output relationship of the neurons in current clamp. Inhibitory interneurons from SOD1 mice were found to have significantly higher threshold voltage than WT interneurons (Fig 3E-F). This shift is likely driven by changes in PICs. Interestingly, despite PIC and threshold changes, the current at firing onset, or I-ON, was not significantly greater in SOD1 interneurons (p = 0.15), similar to the current at firing offset, or I-OFF (p = 0.07) perhaps due to smaller somata in SOD1 interneurons. The AHP also differed in SOD1 interneurons. The duration at half AHP amplitude was shorter in SOD1 neurons, as shown in Fig 3H-I. Amplitude of the AHP was unchanged. While changes in the PIC and threshold indicate less excitability in SOD1 interneurons, the shortened AHP suggests an increased ability to fire at higher rates in SOD1 interneurons, a property that is associated with increased excitability. However, no changes in firing rates were detected in SOD1 interneurons. All other properties were found to be similar in SOD1 and WT glycinergic interneurons, including maximum firing rates, sag/rebound currents (I_H), action potential parameters and membrane properties (see **Table 2** for all electrical properties). See discussion for further interpretation of these findings.

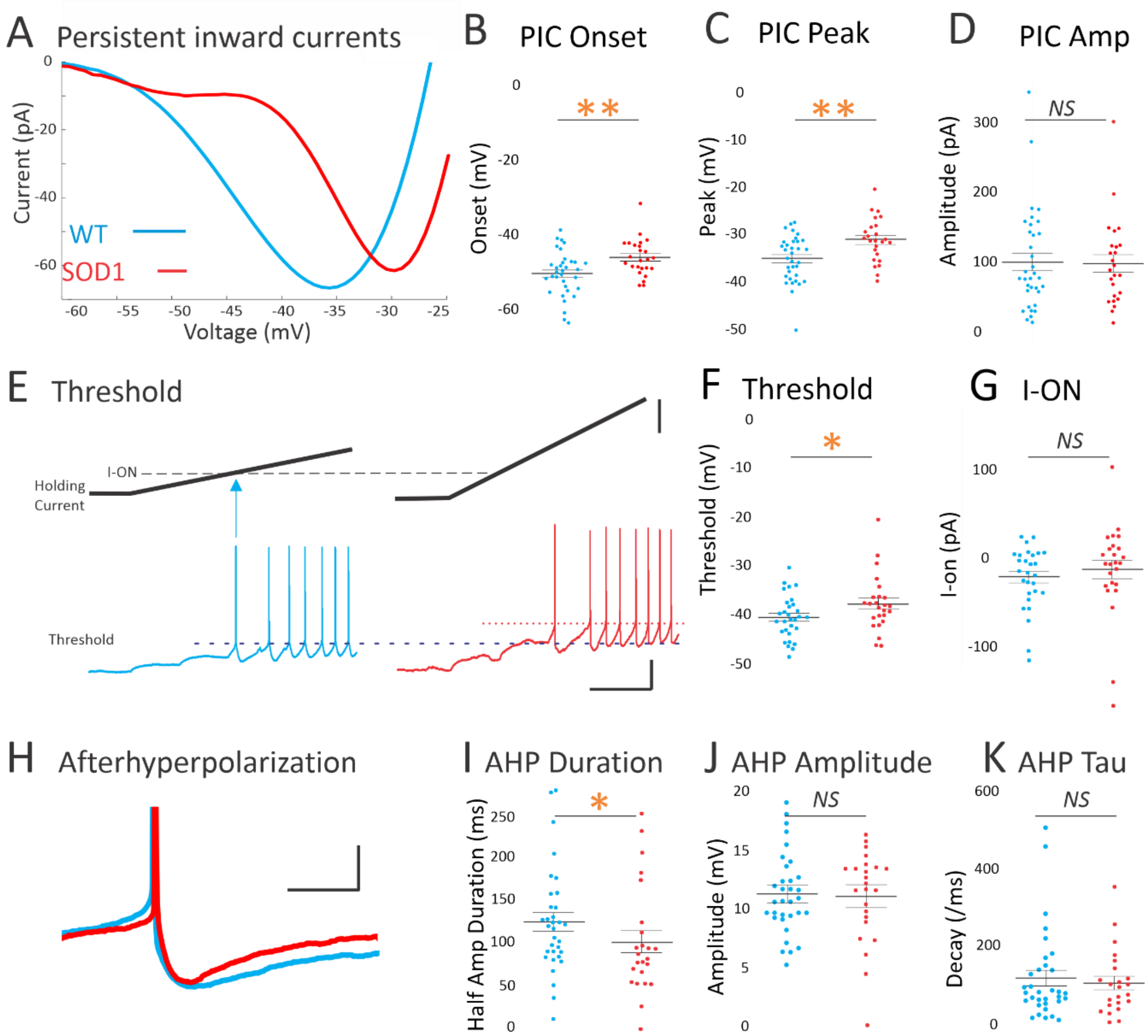

293

Figure 3: Electrophysiology of SOD1 glycinergic interneurons. The most prominent difference in SOD1 interneurons was the shift in voltage dependence of PICs and threshold. (**A**) Representative, leak-subtracted current-voltage relationship of PICs from WT (P8) and SOD1 (P6) interneurons. (**B-D**) Mean onset, peak and amplitude of PICs in WT (blue symbols on left) and SOD1 interneurons (red symbols on right). (**E-F**) Threshold voltage (action potentials evoked with current ramps as shown) was depolarized in SOD1 interneurons (compare dotted lines indicating threshold). Starting potential for both interneurons was -65mV. The current at firing onset (I-ON) was not significantly different as shown in **G.** (**H**) The AHP in SOD1 interneurons was shorter, as shown by the smaller mean duration at half amplitude in a representative P8 WT and P7 SOD1 interneuron and cumulative data in **I.** Neither the AHP amplitude nor the AHP decay time constant, tau, were significantly altered in SOD1 glycinergic interneurons, as shown in **J-K.** Vertical scale bars in **E**: top = 50pA, and bottom = 20mV. Horizontal scale bar in **E** = 0.5s and all scale bars apply to both left and right panels. Vertical scale bar in H = 10mV (APs were truncated from image), and horizontal scale bar = 50ms. Significance denoted with * indicates $p \leq 0.05$; ** indicates $p < 0.01$.

294

Table 2: Electrophysiological properties of GlyT2-GFP+ interneurons in WT and SOD1 animals.

Parameters	**Groups**		
	WT (Mean ± SE)	**SOD (Mean ± SE)**	***p***
	N = 34	*N* = 25	
Resting membrane potential (mV)	-46.7 ± 1.1	-45.7 ± 1.4	0.524[K]
Capacitance (pF)	66 ± 7	55 ± 5	0.529[K]
Input resistance (MΩ)	295 ± 32	299 ± 41	0.794[K]
PIC properties			
PIC onset (mV)	-50.5 ± 1.0	-46.2 ± 1.0**	0.004
PIC peak (mV)	-35.1 ± 0.8	-31.2 ± 0.9**	0.003
PIC amplitude (pA)	100 ± 13	97 ± 12	0.890[K]
Normalized PIC (pA/pF)	1.79 ± 0.24	1.92 ± 0.22	0.226[K]
Firing properties			
Inst firing freq range max (Hz)	112 ± 8	113 ± 8	0.961
Steady state firing freq range min (Hz)	6 ± 0.4	6 ± 0.7	0.453[K]
I-ON (pA)	-55 ± 23	-14 ± 11	0.148[K]
I-OFF (pA)	14 ± 14	36 ± 14	0.074[K]
Δ I (pA)	70 ± 14	50 ± 10	0.331[K]
AP properties			
AP overshoot past 0 (mV)	20.0 ± 1.7	21.4 ± 1.6	0.553
AP duration at half peak (ms)	1.53 ± 0.09	1.48 ± 0.08	0.944
AP rate of rise (V/s)	87 ± 5	83 ± 3	0.428[K]
AP rate of fall (V/s)	45 ± 3	43 ± 2	0.924[K]
Threshold on ramp (mV)	-40.6 ± 0.8	-37.9 ± 1.1*	0.052[K]
Threshold on step (mV)	-47.3 ± 0.8	-45.1 ± 1.3	0.199[K]
AHP properties			
AHP amplitude (mV)	11.2 ± 0.6	11.0 ± 0.8	0.704[K]
AHP duration at half amplitude (s)	0.124 ± 0.010	0.101 ± 0.013*	0.045[K]
AHP tau (s^{-1})	0.117 ± 0.020	0.105 ± 0.017	0.980[K]
I_H properties			
Hyperpolarizing Sag (%)	32 ± 3	32 ± 4	0.537[K]
Depolarizing Rebound (%)	17 ± 3	19 ± 5	0.536[K]

Significance denoted with * indicates $p \leq 0.05$; ** indicates $p < 0.01$.

[K] Indicates Kruskal-Wallis Test for nonparametric distributions; all others were ANOVA analysis.

Regional analysis of glycinergic interneurons

Since ventral glycinergic interneurons are not a homogenous population, we tested for regional differences. Interneurons were divided into three groups based on location 1) the "ventral RC region": within 100 µm of the ventral white matter where Renshaw cells are located, 2) lamina IX, and 3) the "intermediate region": ventral horn region including lamina VII and VIII, excluding the previous two regions. These regions are represented in **Figure 4**. The first region corresponds to the location of RCs (but could contain other types of glycinergic interneurons). The second region contains interneurons that are interspersed with the MNs within the motor pools, likely to be composed of premotor interneurons (more on this in the discussion). The third region contains interneurons that are a mix of premotor interneurons and other classes of ventral interneurons. There was overlap of the first two regions, so interneurons within the ventral most 100 µm that also were located within motor pools were included in both the ventral RC region and lamina IX, as shown in open circles in figure 4.

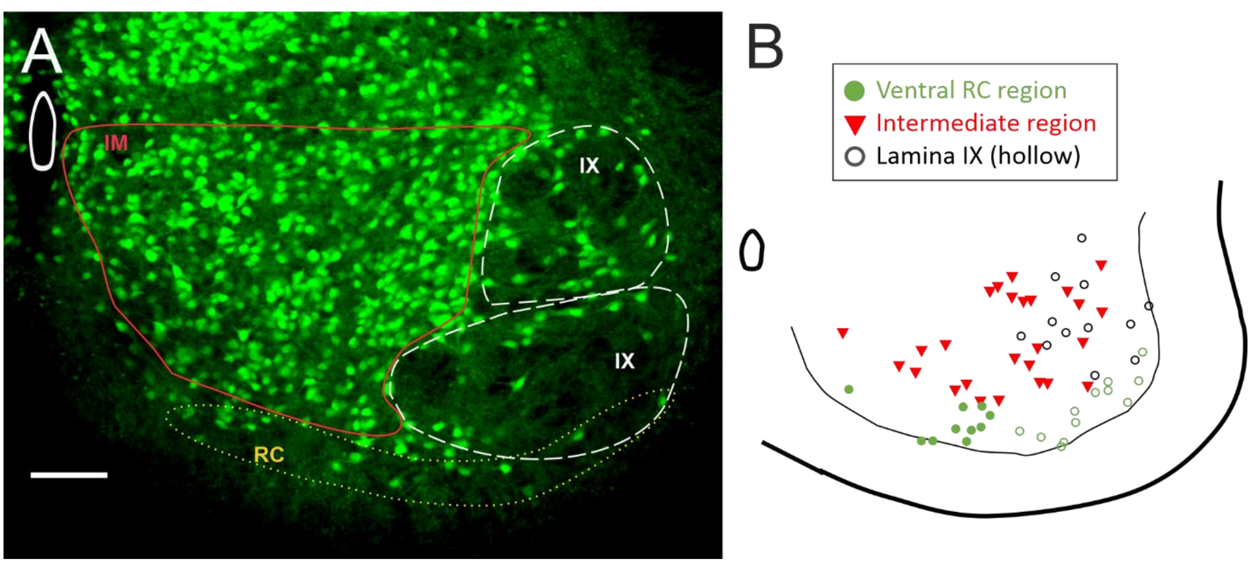

Figure 4: Regional divisions of interneurons. (**A**) Three regions were used for analysis of regional differences in glycinergic interneurons. (**B**) Map of the patched interneurons coded for regions. Ventral region with RC cells (green circles) overlapped with lamina IX (hollow circles). The remaining interneurons that were not within the RC region or lamina IX were grouped into an intermediate region of lamina VII and VIII (red triangles). Scale bar in **A** = 100 µm.

GlyT2 interneurons in Ventral RC region

Within the ventral region where RCs are located, we found that glycinergic SOD1 interneurons there showed the most significant changes in both electrophysiology and morphology. In patch clamped interneurons from this region (N = 8 WT from 7 mice and 13 SOD1 from 9 mice), there was a significant depolarization in PIC onset and peak in glycinergic SOD1 interneurons compared to WT interneurons in the same location. Additionally, primary dendrites were found to be longer and larger in volume and surface area in SOD1 interneurons in the ventral-most 100 µm. Unpatched GlyT2+ SOD1 interneurons in this region (129 WT interneurons from 8 WT mice and 168 SOD1 interneurons from 9 SOD1 mice), analyzed from fixed spinal cords were smaller than WT glycinergic interneurons. These changes (summarized in **Figure 5** and **Table 3**) show that glycinergic neurons in the region where RCs are located are very affected by the SOD1 mutation. For example, primary dendrites of neurons in this region were more altered more significantly than glycinergic interneurons within the entire ventral horn (compare primary dendrite statistics in Tables 1 and 3).

GlyT2 interneurons in Lamina IX

The SOD1 interneurons located in lamina IX, intermixed with MNs were modestly altered in excitability and morphology. As shown in **Figure 6** and **Table 4**, PIC onset was depolarized in SOD1 interneurons in this region, compared to interneurons in this region from WT mice (n = 14 WT interneurons from 8 mice and 11 SOD1 interneurons from 9 mice). Longer total length of primary dendrites was also found in patched interneurons in this region. Within the larger number of unpatched interneurons (345 WT interneurons from 7 WT mice and 306 SOD1 interneurons from 8 SOD1 mice), SOD1 interneurons were found to have smaller somata than WT interneurons.

GlyT2 interneurons in the Intermediate region

The third regional group of glycinergic interneurons was defined as the intermediate region. These interneurons were located in laminae VII and VIII, excluding the ventral 100 µm and lamina IX. Within this area, 16 WT and 8 SOD1 interneurons were patched from 11 WT and 5 SOD1 mice respectively, and 2077 unpatched interneurons were analyzed from 9 WT mice and 1113 unpatched SOD1 interneurons from 9 SOD1 mice. As shown in **Figure 7** and **Table 5**, only PIC peak was significantly depolarized. In unpatched neurons from this region, soma size was significantly smaller in SOD1 interneurons, similar to the other two regions.

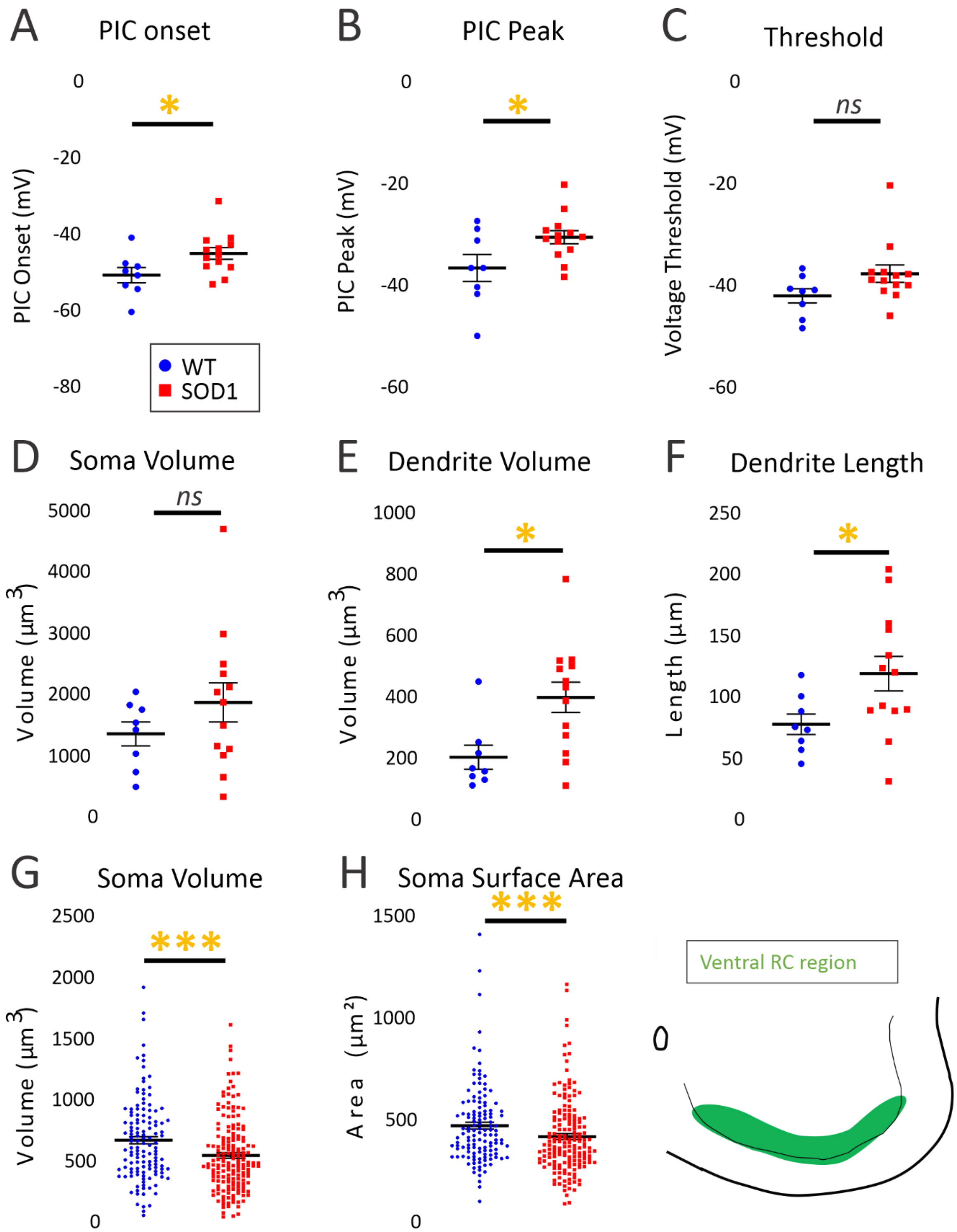

Figure 5: PICs were depolarized in SOD1 GlyT2 interneurons in the ventral RC region. Both onset (**A**) and peak (**B**) of the PIC were depolarized. Threshold was unchanged (**C**). Soma volume of patched neurons (**D**) was unchanged, though SOD1 primary dendrites had more total volume (**E**) and length (**F**) per cell. Larger numbers of unpatched neurons showed smaller soma volume (**G**) and surface area (**H**) in SOD1 interneurons than WT, in RC region. Significance denoted with * indicates $p \leq 0.05$, ** indicates $p \leq 0.01$.

343

344

Table 3: Electrophysiological properties of WT and SOD1 GlyT2-GFP+ interneurons in ventral RC region.

	WT (Mean ± SE)	SOD (Mean ± SE)	*p*
	N = 8	N = 13	
PIC Onset (mV)	-51.3 (± 2.0)	-45.6 (± 1.5) *	0.036
PIC Peak (mV)	-36.8 (± 2.6)	-30.8 (± 1.3) *	0.034
PIC Amplitude (pA)	77.2 (± 15.6)	114.9 (± 19.7)	0.218[K]
I-ON (pA)	-65.6 (± 39.0)	-18.1 (± 14.2)	0.096[K]
I-OFF (pA)	-31.9 (± 20.5)	6.9 (± 15.0)	0.060[K]
Δ I (pA)	36.3 (± 19.4)	25.1 (± 6.8)	0.717[K]
Threshold on ramp (mV)	-42.4 (± 1.4)	-38.0 (± 1.7)	0.070[K]
Threshold on step (mV)	-47.0 (± 1.1)	-44.1 (± 1.6)	0.261[K]
AHP amplitude (mV)	11.6 (± 1.4)	11.4 (± 1.0)	0.921
AHP duration at half amplitude (s)	0.128 (± 0.027)	0.117 (± 0.016)	0.469[K]
AHP tau (s^{-1})	0.117 (± 0.050)	0.109 (± 0.020)	0.346[K]
Morphology of Patched interneurons in RC region			
	N = 8	N = 13	
Soma			
Soma Surface Area (μm²)	589.4 (± 59.0)	700.0 (± 79.1)	0.334
Soma Volume (μm³)	1326.0 (± 195.4)	1841.0 (± 318.8)	0.253
Primary Dendrites			
Total Dendrite Length (μm)	76.4 (± 8.4)	117.7 (± 14.0) *	0.044
Average Dendrite Length (μm)	26.2 (± 2.7)	35.2 (± 3.9)	0.161[K]
Total Dendrite Surface Area (μm²)	407.6 (± 57.3)	680.7 (± 65.7) *	0.010[K]
Average Dendrite Surface Area (μm²)	137.4 (± 14.5)	206.0 (± 21.2) *	0.025[K]
Total Dendrite Volume (μm³)	196.3 (± 38.9)	391.5 (± 49.7) *	0.013[K]
Average Dendrite Volume (μm³)	65.0 (± 9.6)	119.6 (± 16.3) *	0.016[K]
Morphology of Unpatched interneurons in RC region			
	N = 129	N = 168	
Soma Surface Area (μm²)	466.2 (± 17.0)	412.3 (± 14.4) ***	0.000[K]
Soma Volume (μm³)	657.2 (± 29.7)	532.8 (± 23.2) ***	0.000[K]

Significance denoted with * indicates $p \le 0.05$; *** indicates $p < 0.001$.

[K] Indicates Kruskal-Wallis Test for nonparametric distributions; all others were ANOVA analysis.

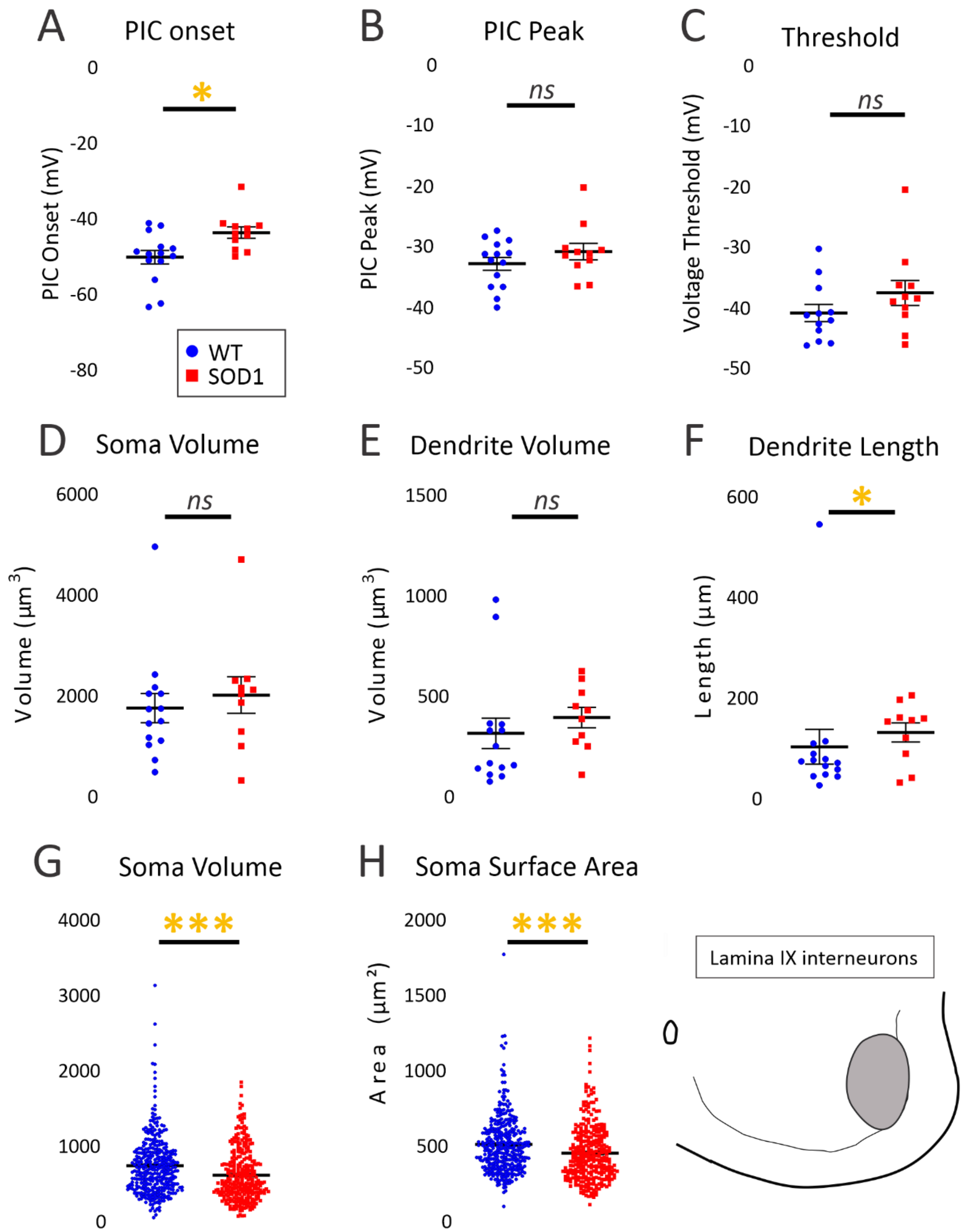

Figure 6: Electrophysiology and morphology was altered in glycinergic SOD1 interneurons in lamina IX. PIC onset (**A**) was depolarized in SOD1 interneurons without changes in PIC peak (**B**) and voltage threshold (**C**). Soma (**D**) and primary dendrite (**E**) total volume was unchanged, but primary dendrite total length was longer (**F**) than in WT interneurons. Unpatched glycinergic neurons showed smaller soma volume (**G**) and surface area (**H**) in SOD1 interneurons than WT in Lamina IX. Significance denoted with * indicates $p \leq 0.05$, *** indicates $p \leq 0.001$.

345

Table 4: Electrophysiological properties of WT and SOD1 GlyT2-GFP+ interneurons in lamina IX.

	WT (Mean ± SE)	SOD (Mean ± SE)	*p*
	N = 14	N = 11	
PIC Onset (mV)	-50.5 (± 1.8)	-44.0 (± 1.5) *	0.013
PIC Peak (mV)	-33.1 (± 1.1)	-31.1 (± 1.4)	0.248
PIC Amplitude (pA)	115.9 (± 21.7)	98.1 (± 22.8)	0.412^{K}
I-ON (pA)	-78.3 (± 47.0)	-11.3 (± 19.3)	0.155^{K}
I-OFF (pA)	21.9 (± 27.9)	22.2 (± 22.0)	0.250^{K}
Δ I (pA)	101.7 (± 73.1)	33.4 (± 9.0)	0.701
Threshold on ramp (mV)	-41.1 (± 1.4)	-37.8 (± 2.1)	0.193
Threshold on step (mV)	-47.4 (± 1.1)	-43.9 (± 2.2)	0.112^{K}
AHP amplitude (mV)	11.4 (± 1.0)	10.2 (± 1.0)	0.421
AHP duration at half amplitude (s)	0.125 (± 0.019)	0.094 (± 0.019)	0.139^{K}
AHP tau (s^{-1})	0.129 (± 0.032)	0.076 (± 0.032)	0.274^{K}
Morphology of Patched interneurons in lamina IX			
	N = 14	N = 10	
Soma			
Soma Surface Area (µm²)	702.6 (± 64.8)	734.3 (± 89.8)	0.771
Soma Volume (µm³)	1731.2 (± 288.6)	1988.8 (± 363.2)	0.412^{K}
Primary Dendrites			
Total Dendrite Length (µm)	100.8 (± 34.6)	129.3 (± 18.9) *	0.046^{K}
Average Dendrite Length (µm)	29.3 (± 6.5)	36.7 (± 5.0)	0.069^{K}
Total Dendrite Surface Area (µm²)	544.8 (± 140.1)	721.5 (± 92.8)	0.089^{K}
Average Dendrite Surface Area (µm²)	164.0 (± 26.3)	208.0 (± 25.2)	0.128^{K}
Total Dendrite Volume (µm³)	308.8 (± 75.5)	387.6 (± 51.0)	0.114^{K}
Average Dendrite Volume (µm³)	94.9 (± 17.5)	113.3 (± 14.5)	0.178^{K}
Morphology of Unpatched interneurons in lamina IX			
	N = 345	N = 306	
Soma Surface Area (µm²)	505.9 (± 10.4)	448.3 (± 10.7) ***	0.000^{K}
Soma Volume (µm³)	732.0 (± 21.1)	605.1 (± 19.6) ***	0.000^{K}

Significance denoted with * indicates $p \leq 0.05$; *** indicates $p < 0.001$.

^{K} Indicates Kruskal-Wallis Test for nonparametric distributions; all others were ANOVA analysis.

350

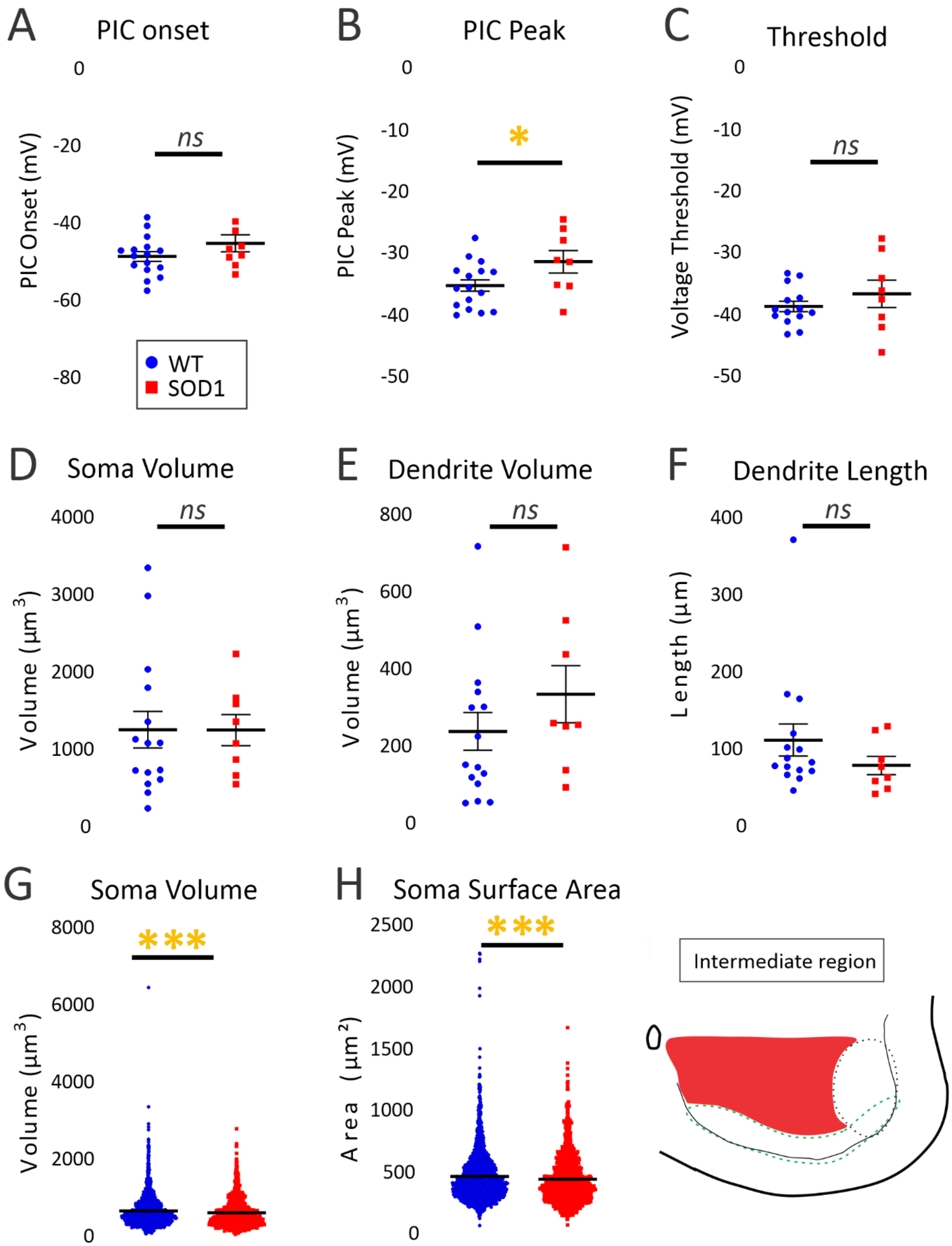

Figure 7: Morphology was altered in SOD1 interneurons in the intermediate regions of laminae VII and VIII. PIC onset (**A**) was not significantly different in SOD1 interneurons, though PIC peak (**B**) was depolarized. Voltage threshold (**C**) was not affected. Morphology of soma (**D**) and dendrites (**E** and **F**) in patched SOD1 interneurons were unchanged, however larger numbers of unpatched neurons showed smaller soma volume (**G**) and surface area (**H**) in SOD1 interneurons than in WT, in laminas VII and VIII. Significance denoted with * indicates $p \leq 0.05$, *** indicates $p \leq 0.001$.

Table 5: Electrophysiological properties of WT and SOD1 GlyT2-GFP+ interneurons in Intermediate Region of lamina VII and VIII.

Parameters	**Groups**		
	WT (Mean ± SE)	**SOD (Mean ± SE)**	***p***
	N = 16	N = 8	
PIC Onset (mV)	-49.0 (± 1.3)	-47.4 (± 1.6)	0.435
PIC Peak (mV)	-35.5 (± 0.9)	-31.7 (± 1.8) *	0.046
PIC Amplitude (pA)	92.1 (± 16.7)	77.0 (± 17.7)	0.881[K]
I-ON (pA)	-18.2 (± 11.6)	-16.5 (± 19.1)	0.776[K]
I-OFF (pA)	20.9 (± 12.2)	73.9 (± 26.7)	0.101[K]
Δ I (pA)	39.0 (± 9.1)	69.1 (± 24.4)	0.076[K]
Threshold on ramp (mV)	-38.9 (± 0.83)	-37.0 (± 2.2)	0.525[K]
Threshold on step (mV)	-46.7 (± 1.2)	-46.3 (± 2.4)	0.490[K]
AHP amplitude (mV)	11.3 (± 0.8)	10.5 (± 2.0)	0.658
AHP duration at half amplitude (s)	0.116 (± 0.011)	0.095 (± 0.030)	0.267[K]
AHP tau (s^{-1})	0.119 (± 0.032)	0.127 (± 0.051)	1.000[K]
Morphology of Patched interneurons in laminae VII and VIII.			
	N = 15	N = 8	
Soma			
Soma Surface Area (μm^2)	573.5 (± 62.9)	558.5 (± 56.7)	0.699[K]
Soma Volume (μm^3)	1232.3 (± 237.4)	1228.2 (± 201.6)	0.776[K]
Primary Dendrites			
Total Dendrite Length (μm)	109.7 (± 20.7)	76.7 (± 11.7)	0.220[K]
Average Dendrite Length (μm)	30.2 (± 4.8)	24.5 (±2.7)	0.606[K]
Total Dendrite Surface Area (μm^2)	505.5 (± 83.0)	513.7 (± 93.6)	0.699[K]
Average Dendrite Surface Area (μm^2)	138.9 (± 18.7)	168.0 (± 30.1)	0.366[K]
Total Dendrite Volume (μm^3)	233.9 (± 48.8)	330.4 (± 74.1)	0.272[K]
Average Dendrite Volume (μm^3)	64.1 (±11.8)	108.8 (±24.8)	0.071[K]
Morphology of Unpatched interneurons in laminae VII and VIII.			
	N = 2077	N = 1113	
Soma Surface Area (μm^2)	451.7 (± 4.6)	428.3 (± 5.9) ***	0.000[K]
Soma Volume (μm^3)	624.9 (± 9.0)	575.3 (± 11.4) ***	0.000[K]

Significance denoted with * indicates $p \leq 0.05$; *** indicates $p < 0.001$.

[K] Indicates Kruskal-Wallis Test for nonparametric distributions; all others were ANOVA analysis.

Taken together, these results show that glycinergic interneurons are profoundly affected by the SOD1 mutation and are altered very early in life in both electrophysiology and morphology. These changes appear to be more severe in very ventrally located interneurons.

Discussion

This study shows for the first time that glycinergic interneurons are depressed in excitability in the SOD1 mouse model and may be contributing to ALS pathology. Alterations in both morphology and excitability of glycinergic interneurons occur at a very early, presymptomatic stage, and are particularly prominent those interneurons located within 100 µm of the ventral white matter. We speculate that these shifts in interneuron excitability and morphology could have functional consequences that alter inhibition of MNs, modify motor output, and could even provide an early biomarker of ALS.

Intrinsic and synaptic hyperexcitability

A core issue this study brings to light is potential long-term disruption to the balance of excitatory and inhibitory synaptic transmission in ALS. Spinal cord and cortex both show an imbalance between excitatory and inhibitory synaptic transmission in SOD^{G93A} mice (Avossa et al., 2006; Saba et al., 2016). Clinically, ALS patients show evidence of altered synaptic activity as well, including a reduction in inhibition. A reduction of glycinergic receptor binding in the anterior gray matter of the spinal cord (Hayashi et al., 1981; Whitehouse et al., 1983) has been demonstrated along with abnormal glycine and gamma amino butyric acid (GABA) levels in blood serum (Malessa et al., 1991; Niebroj-Dobosz and Janik, 1999). Electrophysiology also suggests disruption in spinal inhibitory circuits in ALS patients (Raynor and Shefner, 1994; Shefner and Logigian, 1998; Sangari et al., 2016; Özyurt et al., 2020). An interesting question is whether the neurons are altered in excitability only within the motor circuit (i.e., corticospinal neurons and the synaptically-connected spinal inhibitory and cholinergic interneurons, and MNs), or if disturbances are more widespread throughout the nervous system. In the spinal cord, interneurons that serve as conduits between vulnerable corticospinal and spinal MNs include cholinergic interneurons, Ia inhibitory interneurons and RCs. There is abundant evidence of disruption in these cholinergic, GABAergic and glycinergic synapses from animal models (Martin et al., 2007; Chang and Martin, 2009b; Pullen and Athanasiou, 2009; Hossaini et al., 2011; Herron and Miles, 2012; Casas et al., 2013; Wootz et al., 2013; Saxena et al., 2013; Milan et al., 2015; Dukkipati et al., 2016; Medelin et al., 2016). Similarly, in the cortex, neurons that are not themselves vulnerable to neurodegeneration in ALS also exhibit altered excitability and morphology in a parallel time course to the vulnerable corticospinal neurons (Clark et al., 2017, 2018; Kim et al., 2017). The changes in excitability of other neuronal populations must contribute to the imbalance of both excitatory and inhibitory neurotransmission that has been clearly demonstrated in ALS patients and animal models.

A case for hyperexcitability and glutamate excitotoxicity in ALS pathogenesis has been more controversial. Altered intrinsic excitability has been consistently reported in both corticospinal projection neurons and spinal MNs, but these perturbations appear to fluctuate based on age/disease progression. Corticospinal projection neurons have increased firing and other signs of hyperexcitability during the first week of postnatal development (Pieri et al., 2009; Saba et al., 2016, 2019; Kim et al., 2017), but excitability is normal in young and adult pre-symptomatic ages (Kim et al., 2017; Saba et al., 2019), and may become hypoexcitable at the age of symptom onset (Saba et al., 2019). Similarly, spinal MNs show intrinsic hyperexcitability at very early (embryonic) stages (Kuo et al., 2004, 2005; Martin et al., 2013). At a postnatal age similar to the inhibitory interneurons in this study, spinal MNs do *not* have an altered threshold, rheobase or frequency-current relationship, though other abnormalities are present in PICs, action potential duration, AHP and dendritic Ca^{2+} entry (Pambo-Pambo et al., 2009; Quinlan et al., 2011, 2015; Leroy et al., 2014). Thus, at the age studied here, *inhibitory interneurons are more disrupted in excitability than the vulnerable spinal MNs*. At symptom onset, MNs may finally succumb to hypoexcitability, though not all studies agree on this point (Delestrée et al., 2014; Martinez-Silva et al., 2018; Jensen et al., 2020). Notably, MNs derived from ALS patients' induced pluripotent stem cells also show initial hyperexcitability followed by hypoexcitability (Wainger et al., 2014; Devlin et al., 2015), and increasing excitability of MNs enhanced neuroprotection rather than neurodegeneration (Saxena et al., 2013). A unifying theme throughout the findings is that vulnerable MNs show excessive homeostatic gain in response to perturbation (Kuo et al., 2020), and not only excitability but other cellular properties fluctuate over the lifespan of the animal (Irvin et al., 2015). In light of that, whether inhibitory interneurons are less excitable at other ages should be explored in future studies to fully characterize their contribution to neurodegenerative processes.

Changes in neuron morphology

In ALS models, altered morphology in spinal MNs occurs so early that it could be viewed as a deficit in normal development. Embryonically, SOD1 MNs have shorter projections but this is reversed during postnatal development. At 1-2 weeks of age, SOD1 MNs begin to show more dendritic branching and larger soma sizes than WT MNs (Amendola and Durand, 2008; Filipchuk and Durand, 2012; Martin et al., 2013). Interestingly, this could be caused by lack of inhibitory input to MNs (Fogarty et al., 2016). SOD1 spinal MNs remain larger than WT MNs through adulthood (Dukkipati et al., 2018). In contrast to the spinal MNs at this age, we found that SOD1 inhibitory interneurons had smaller soma size and yet had expanded dendritic surface area and volume of primary dendrites compared to WT glycinergic interneurons. This is reminiscent of changes in corticospinal neurons: presymptomatic corticospinal neurons also have increased arborization but with smaller soma diameters (Ozdinler et al., 2011; Saba et al., 2016). In both sporadic and familial ALS patients, postmortem tissue shows degeneration of apical dendrites in corticospinal neurons and smaller soma size (Genç et al., 2017). In SOD1 spinal interneurons in the present study, increased dendrite length, surface area and volume of primary dendrites was most prominent in the ventral interneurons in the RC region, while smaller soma sizes were found throughout the ventral horn. Altered neuronal size / arborization could alter the impact of other stressors (e.g., proteostasis, metabolic deficits, intracellular transport).

After spike afterhyperpolarization

The AHP can contribute to a neuron's firing rate such that a neuron with a large, long-lasting AHP will typically fire at a slower rate (typical of slow/type I MNs) than a neuron with small, fast-decaying AHP (typical of fast/type II MNs). In ALS patients, the AHP is shortened in MNs of patients with little force deficits and later elongated in patients with large force deficits (Piotrkiewicz and Hausmanowa-Petrusewicz, 2011), which could reflect early changes in physiology of vulnerable fast MNs and later, the remaining, less-vulnerable population of slow MNs. Similarly, SOD1 mouse MNs show shorter AHPs early, and longer AHPs around symptom onset (Quinlan et al., 2011; Jensen et al., 2020). Here we show that AHP is shorter in duration in SOD1 interneurons very early in life. In the regional analysis, AHP parameters were not found to be significantly altered in any of the 3 regions, but it is possible this was due to a loss in statistical power in the smaller groups. We did not find concomitant changes in minimum or maximum firing rates in GlyT2 interneurons, so the physiological importance of the altered AHP duration in interneurons is unclear.

Inhibitory interneurons: Subtype specific effects

The interneurons in this study were heterogenous, and based on their location and electrophysiology, they likely were composed of V1 and V2b interneurons including RCs, commissural interneurons (V2b interneurons), and Ia inhibitory interneurons, and perhaps inhibitory propriospinal interneurons (Willis and Willis, 1964; Restrepo et al., 2009; Bikoff et al., 2016; Flynn et al., 2017). Because of this heterogeneity, interneurons were separated into regions for further analysis, to examine more specifically which inhibitory interneurons were perturbed. Based on our regional analysis, interneurons in the ventral-most 100 µm from white matter were altered the most in both excitability and morphology, with the most strongly depolarized PICs and larger primary dendrites, moreso than glycinergic interneurons within lamina IX and intermediate lamina VI and VII. Interneurons located in the region within 100 µm from the ventral white matter likely contain more RCs based on the location (Siembab et al., 2010) and electrophysiological characteristics (Perry et al., 2015; Bikoff et al., 2016). Glycinergic interneurons located in lamina IX are reminiscent of the locomotor-related GABAergic interneurons characterized by Nishimaru and colleagues, which were located within the ventrolateral spinal cord, surrounded MNs and were active during locomotor activity (Nishimaru et al., 2011). Indeed these may be the same neurons: colocalization of GABA and glycine is entirely possible (Jonas et al., 1998; Allain et al., 2006). If the lamina IX interneurons are indeed locomotor-related, even a modest dampening of excitability observed here in SOD1 mice could contribute to changes in locomotor patterning as has been described in other studies (Quinlan et al., 2017; Allodi et al., 2021). Further studies are warranted to examine how inhibitory interneurons may be differently modulated in a subtype-specific manner in animal models of ALS.

Functional implications for impaired inhibitory circuits

Outward signs of improperly functioning inhibitory interneurons may be apparent from subtle changes in motor patterning and could potentially be used as a biomarker of early ALS. Locomotor disturbances have been demonstrated *in vivo* in presymptomatic SOD1 mice during walking/running (Vinsant et al., 2013; Akay, 2014; Quinlan et al., 2017; Allodi et al., 2021). In the embryonic and neonatal spinal cord *in vitro*, increased duration of depolarizing events in MNs and a slower period of locomotor-related bursting has been described (Medelin et al., 2016; Branchereau et al., 2019), which indicate that even during development the functioning of locomotor circuits is already impaired. In presymptomatic adult mice capable of running on a treadmill, subtle locomotor differences are observed including advanced intermuscular phasing and a slower speed (Quinlan et al., 2017; Allodi et al., 2021) which indicate that before any large scale neurodegeneration occurs, there are changes in patterns of activity in MNs and interneurons that could be exploited for use as a biomarker of ALS. At initial symptom onset, the first failure of the tibialis anterior manifests as abnormality in the swing phase of the ankle (Akay, 2014). Interestingly, silencing different interneuron populations (including inhibitory interneurons and cholinergic interneurons) reveals the contribution of each population: silencing cholinergic interneurons increases locomotor deficits in SOD1 mice (Landoni et al., 2019), while silencing inhibitory interneurons has no effect suggesting these interneurons are already impaired (Allodi et al., 2021).

Clinical-translational implications

Evidence of MN hyperexcitability in ALS patients is present alongside signs of dysfunction in inhibition (Rothstein et al., 1992; Plaitakis and Constantakakis, 1993; Raynor and Shefner, 1994; Shefner and Logigian, 1998; Andreadou et al., 2008; Bae et al., 2013). Perhaps reducing excitability (with riluzole, for example) only results in a modest increase in lifespan (Bensimon et al., 1994) because it could be helpful to MNs while exacerbating inhibitory dysfunction by further depressing excitability of inhibitory interneurons like RCs. Thus, a more targeted approach to reduce MN excitability could be beneficial early in disease pathology. Stimulation of inhibitory nerves or certain protocols of transcranial stimulation could be explored, along with augmentation of inhibitory neurotransmission.

Data Availability Statement

All data presented in this article were included in the Figures and Tables. Data were excluded only based on the criteria stated in the methods.

Competing interests

Authors have no competing interests/conflicts of interest.

Author contributions

CFC: acquisition of imaging data, analysis of 3D reconstruction data, statistics and writing the manuscript
PRS: analysis of electrophysiology and statistical data, and revising the manuscript
LMM: analysis of statistical data, revising the manuscript
KJL: analysis of 3D reconstruction data, revising the manuscript
ACP: analysis of electrophysiology data, revising the manuscript

NK: conception and design of the work, revising the manuscript

KAQ: conception and design of the work, acquisition of electrophysiology and imaging data, analysis of electrophysiological data, statistics and writing the manuscript

All authors approved the final version of the manuscript; agreed to be accountable for all aspects of the work in ensuring that questions related to the accuracy or integrity of any part of the work are appropriately investigated and resolved; and all persons designated as authors qualify for authorship, and all those who qualify for authorship are listed.

Funding

This project was funded by a springboard fellowship from Target ALS to KAQ and a University of Rhode Island Graduate School Tuition Scholarship to LMM.

Acknowledgments

The authors made use of equipment supported by the Institutional Development Award (IDeA) Network for Biomedical Research Excellence from the National Institute of General Medical Sciences of the National Institutes of Health under grant number P20GM103430. The authors thank Drs. Emily Reedich, Claudia Fallini and Marin Manuel for comments on the initial drafts of the manuscript.

References

Akay T (2014) Long-term measurement of muscle denervation and locomotor behavior in individual wild-type and ALS model mice. J Neurophysiol 111:694–703.

Allain A-E, Bairi A, Meyrand P, Branchereau P (2006) Expression of the Glycinergic System During the Course of Embryonic Development in the Mouse Spinal Cord and its Co-Localization with GABA Immunoreactivity. J Comp Neurol 496:832–846.

Allodi I, Montañana-Rosell R, Selvan R, Löw P, Kiehn O (2021) Locomotor deficits in a mouse model of ALS are paralleled by loss of V1-interneuron connections onto fast motor neurons. Nat Commun 12:1–18 Available at: http://dx.doi.org/10.1038/s41467-021-23224-7.

Amendola J, Durand J (2008) Morphological differences between wild-type and transgenic superoxide dismutase 1 lumbar motoneurons in postnatal mice. J Comp Neurol 511:329–341.

Andreadou E, Kapaki E, Kokotis P, Paraskevas GP, Katsaros N, Libitaki G, Petropoulou O, Zis V, Sfagos C, Vassilopoulos D (2008) Plasma glutamate and glycine levels in patients with amyotrophic lateral sclerosis. In Vivo (Brooklyn) 22:137–142.

Avossa D, Grandolfo M, Mazzarol F, Zatta M, Ballerini L (2006) Early signs of motoneuron vulnerability in a disease model system: Characterization of transverse slice cultures of spinal cord isolated from embryonic ALS mice. Neuroscience 138:1179–1194.

Bae JS, Simon NG, Menon P, Vucic S, Kiernan C, Doyle AC, Case-book T, Holmes S (2013) The Puzzling Case of Hyperexcitability in Amyotrophic Lateral Sclerosis What Really is Hyperexcitability in ALS ? How Can We Objectively Assess. J Clin Neurol 9:65–74.

Bensimon G, Lacomblez L, Meininger V (1994) A Controlled Trial of Riluzole in Amyotrophic Lateral Sclerosis. N Engl J Med 330:585–591.

Bikoff JB, Gabitto MI, Rivard AF, Drobac E, Machado TA, Miri A, Brenner-Morton S, Famojure E, Diaz C, Alvarez FJ, Mentis GZ, Jessell TM (2016) Spinal Inhibitory Interneuron Diversity Delineates Variant Motor Microcircuits. Cell 165:207–219 Available at: http://www.embase.com/search/results?subaction=viewrecord&from=export&id=L608793625%0Ahttp://dx.doi.org/10.1016/j.cell.2016.01.027.

Branchereau P, Martin E, Supiot L, Hodeib F, Laupénie A, Dalvi U, Zhu H, Cazenave W, Cattaert D (2019) Relaxation of synaptic inhibitory events as a compensatory mechanism in fetal SOD spinal motor networks. Elife 8:1–28.

Casas C, Herrando-Grabulosa M, Manzano R, Mancuso R, Osta R, Navarro X (2013) Early presymptomatic cholinergic dysfunction in a murine model of amyotrophic lateral sclerosis. Brain Behav 3:145–158.

Chang Q, Martin LJ (2009a) Glycinergic Innervation of Motoneurons Is Deficient in Amyotrophic Lateral Sclerosis Mice A Quantitative Confocal Analysis. Am J Pathol 174:574–585.

Chang Q, Martin LJ (2009b) Glycinergic innervation of motoneurons is deficient in amyotrophic lateral sclerosis mice: A quantitative confocal analysis. Am J Pathol 174:574–585.

Clark RM, Blizzard CA, Young KM, King AE, Dickson TC (2017) Calretinin and Neuropeptide y interneurons are differentially altered in the motor cortex of the SOD1 G93A mouse model of ALS. Sci Rep 7:1–13 Available at: http://dx.doi.org/10.1038/srep44461.

Clark RM, Brizuela M, Blizzard CA, Dickson TC (2018) Reduced excitability and increased neurite complexity of cortical interneurons in a familial mouse model of amyotrophic lateral sclerosis. Front Cell Neurosci 12:1–7.

Delestrée N, Manuel M, Iglesias C, Elbasiouny SM, Heckman CJ, Zytnicki D (2014) Adult spinal motoneurones are not hyperexcitable in a mouse model of inherited amyotrophic lateral sclerosis. J Physiol 592:1687–1703.

Devlin AC, Burr K, Borooah S, Foster JD, Cleary EM, Geti I, Vallier L, Shaw CE, Chandran S, Miles GB (2015) Human iPSC-derived motoneurons harbouring TARDBP or C9ORF72 ALS mutations are dysfunctional despite maintaining viability. Nat Commun 6:1–12 Available at: http://dx.doi.org/10.1038/ncomms6999.

Dukkipati SS, Chihi A, Wang Y, Elbasiouny SM (2016) Experimental Design and Data Analysis Issues Contribute to Inconsistent Results of C-Bouton Changes in Amyotrophic Lateral Sclerosis. eNeuro 4:1–13.

Dukkipati SS, Garrett TL, Elbasiouny SM (2018) The vulnerability of spinal motoneurons and soma size plasticity in a mouse model of amyotrophic lateral sclerosis. J Physiol 596:1723–1745.

Filipchuk AA, Durand J (2012) Postnatal dendritic development in lumbar motoneurons in mutant superoxide dismutase 1 mouse model of amyotrophic lateral sclerosis. Neuroscience 209:144–154 Available at: http://dx.doi.org/10.1016/j.neuroscience.2012.01.046.

Flynn JR, Conn VL, Boyle KA, Hughes DI, Watanabe M, Velasquez T, Goulding MD, Callister RJ, Graham BA (2017) Anatomical and molecular properties of long descending propriospinal neurons in mice. Front Neuroanat 11:1–13.

Fogarty MJ, Kanjhan R, Bellingham MC, Noakes PG (2016) Glycinergic neurotransmission: A potent regulator of embryonic motor neuron dendritic morphology and synaptic plasticity. J Neurosci 36:80–87.

Genç B, Jara JH, Lagrimas AKB, Pytel P, Roos RP, Mesulam MM, Geula C, Bigio EH, Özdinler PH (2017) Apical dendrite degeneration, a novel cellular pathology for Betz cells in ALS. Sci Rep 7:1–10 Available at: http://dx.doi.org/10.1038/srep41765.

Gunes ZI, Kan VWY, Ye XQ, Liebscher S (2020) Exciting Complexity: The Role of Motor Circuit Elements in ALS Pathophysiology. Front Neurosci 14:1–30.

Hayashi H, Suga M, Satake M, Tsubaki T (1981) Reduced glycine receptor in the spinal cord in amyotrophic lateral sclerosis. Ann Neurol 9:292–294.

Hegedus J, Putman CT, Gordon T (2007) Time course of preferential motor unit loss in the SOD1G93A mouse model of amyotrophic lateral sclerosis. Neurobiol Dis 28:154–164.

Herron LR, Miles GB (2012) GENDER-SPECIFIC PERTURBATIONS IN MODULATORY INPUTS TO MOTONEURONS IN A MOUSE MODEL OF AMYOTROPHIC LATERAL SCLEROSIS. Neuroscience 226:313–323 Available at: http://dx.doi.org/10.1016/j.neuroscience.2012.09.031.

Hossaini M, Cano SC, Van Dis V, Haasdijk ED, Hoogenraad CC, Holstege JC, Jaarsma D (2011) Spinal inhibitory interneuron pathology follows motor neuron degeneration independent of glial mutant superoxide dismutase 1 expression in SOD1-ALS mice. J Neuropathol Exp Neurol 70:662–677.

Howells J, Sangari S, Matamala JM, Kiernan MC, Marchand-Pauvert V, Burke D (2020) Interrogating interneurone function using threshold tracking of the H reflex in healthy subjects and patients with motor neurone disease. Clin Neurophysiol 131:1986–1996.

Irvin CW, Kim RB, Mitchell CS (2015) Seeking homeostasis: Temporal trends in respiration, oxidation, and calcium in SOD1 G93A amyotrophic lateral sclerosis mice. Front Cell Neurosci 9:1–11.

Jensen DB, Kadlecova M, Allodi I, Meehan CF (2020) Spinal motoneurones are intrinsically more responsive in the adult G93A SOD1 mouse model of Amyotrophic Lateral Sclerosis. J Physiol.

Jonas P, Bischofberger J, Sandkühler J (1998) Corelease of two fast neurotransmitters at a central synapse. Science (80-) 281:419–424.

Kim J, Hughes EG, Shetty AS, Arlotta P, Goff LA, Bergles DE, Brown SP (2017) Changes in the Excitability of Neocortical Neurons in a Mouse Model of Amyotrophic Lateral Sclerosis Are Not Specific to Corticospinal Neurons and Are Modulated by Advancing Disease. J Neurosci 37:9037–9053 Available at: http://www.jneurosci.org/lookup/doi/10.1523/JNEUROSCI.0811-17.2017.

Kuo JJ, Schonewille M, Siddique T, Schults AN, Fu R, Bar PR, Anelli R, Heckman C, Kroese AB (2004) Hyperexcitability of Cultured Spinal Motoneurons From Presymptomatic ALS Mice. J Neurophysiol 91:571–575 Available at: http://jn.physiology.org/cgi/doi/10.1152/jn.00665.2003.

Kuo JJ, Siddique T, Fu R, Heckman CJ (2005) Increased persistent Na+ current and its effect on excitability in motoneurones cultured from mutant SOD1 mice. J Physiol 563:843–854.

Kuo SW, Binder MD, Heckman CJ (2020) Excessive Homeostatic Gain in Spinal Motoneurons in a Mouse Model of Amyotrophic Lateral Sclerosis. Sci Rep 10.

Landoni LM, Myles JR, Wells TL, Mayer WP, Akay T (2019) Cholinergic modulation of motor neurons through the C-boutons are necessary for the locomotor compensation for severe motor neuron loss during amyotrophic lateral sclerosis disease progression. Behav Brain Res 369.

Leroy F, Lamotte d'Incamps B, Imhoff-Manuel RD, Zytnicki D (2014) Early intrinsic hyperexcitability does not contribute to motoneuron degeneration in amyotrophic lateral sclerosis. Elife 3:1–25.

Malessa S, Leigh PN, Bertel O, Sluga E, Hornykiewicz O (1991) Amyotrophic lateral sclerosis: glutamate dehydrogenase and transmitter amino acids in the spinal cord. J Neurol Neurosurg Psychiatry 54:984–988.

Martin E, Cazenave W, Cattaert D, Branchereau P (2013) Embryonic alteration of motoneuronal morphology induces hyperexcitability in the mouse model of amyotrophic lateral sclerosis. Neurobiol Dis 54:116–126.

Martin LJ, Liu Z, Chen K, Price AC, Pan Y, Swaby JA, Golden WC (2007) Motor Neuron Degeneration in Amyotrophic Lateral Sclerosis Mutant Superoxide Dismutase-1 Transgenic Mice: Mechanisms of Mitochondriopathy and Cell Death. J Comp Neurol 500:20–46.

Martinez-Silva M de L, Imhoff-Manuel RD, Sharma A, Heckman C, Shneider NA, Roselli F, Zytnicki D, Manuel M (2018) Hypoexcitability precedes denervation in the large fast-contracting motor units in two unrelated mouse models of ALS. Elife 7:1–26.

McGown A, McDearmid JR, Panagiotaki N, Tong H, Al Mashhadi S, Redhead N, Lyon AN, Beattie CE, Shaw PJ, Ramesh TM (2013) Early interneuron dysfunction in ALS: Insights from a mutant sod1 zebrafish model. Ann Neurol 73:246–258.

Medelin M, Rancic V, Cellot G, Laishram J, Veeraraghavan P, Rossi C, Muzio L, Sivilotti L, Ballerini L (2016) Altered development in GABA co-release shapes glycinergic synaptic currents in cultured spinal slices of the SOD1G93Amouse model of amyotrophic lateral sclerosis. J Physiol 594:3827–3840.

Milan L, Courtand G, Cardoit L, Masmejean F, Barrière G, Cazalets JR, Garret M, Bertrand SS (2015) Age-related changes in pre- and postsynaptic partners of the cholinergic C-boutons in wild-type and SOD1G93Alumbar motoneurons. PLoS One 10:1–21.

Niebroj-Dobosz I, Janik P (1999) Amino acids acting as transmitters in amyotrophic lateral sclerosis (ALS).

Acta Neurol Scand 100:6–11.

Nishimaru H, Sakagami H, Kakizaki M, Yanagawa Y (2011) Locomotor-related activity of GABAergic interneurons localized in the ventrolateral region in the isolated spinal cord of neonatal mice. J Neurophysiol 106:1782–1792.

Ozdinler PH, Benn S, Yamamoto TH, Guzel M, Brown RH, Macklis JD (2011) Corticospinal Motor Neurons and Related Subcerebral Projection Neurons Undergo Early and Specific Neurodegeneration in hSOD1G93A Transgenic ALS Mice. J Neurosci 31:4166–4177 Available at: http://www.jneurosci.org/cgi/doi/10.1523/JNEUROSCI.4184-10.2011.

Özyurt MG, Topkara B, İşak B, Türker KS (2020) Amyotrophic lateral sclerosis weakens spinal recurrent inhibition and post-activation depression. Clin Neurophysiol 131:2875–2886.

Pambo-Pambo A, Durand J, Gueritaud J-P (2009) Early excitability changes in lumbar motoneurons of transgenic SOD1G85R and SOD1G(93A-Low) mice. J Neurophysiol 102:3627–3642 Available at: http://www.ncbi.nlm.nih.gov/pubmed/19828728.

Perry S, Gezelius H, Larhammar M, Hilscher MM, Lamotte d'Incamps B, Leao KE, Kullander K (2015) Firing properties of Renshaw cells defined by Chrna2 are modulated by hyperpolarizing and small conductance ion currents I<inf>h</inf> and I<inf>SK</inf>. Eur J Neurosci 41:887–898.

Pieri M, Carunchio I, Curcio L, Mercuri NB, Zona C (2009) Increased persistent sodium current determines cortical hyperexcitability in a genetic model of amyotrophic lateral sclerosis. Exp Neurol 215:368–379 Available at: http://dx.doi.org/10.1016/j.expneurol.2008.11.002.

Piotrkiewicz M, Hausmanowa-Petrusewicz I (2011) Motoneuron afterhyperpolarisation duration in amyotrophic lateral sclerosis. J Physiol 589:2745–2754.

Plaitakis A, Constantakakis E (1993) Altered metabolism of excitatory amino acids, N-acetyl-aspartate and N-acetyl-aspartylglutamate in amyotrophic lateral sclerosis. Brain Res Bull 30:381–386.

Pullen AH, Athanasiou D (2009) Increase in presynaptic territory of C-terminals on lumbar motoneurons of G93A SOD1 mice during disease progression. Eur J Neurosci 29:551–561.

Pun S, Santos AF, Saxena S, Xu L, Caroni P (2006) Selective vulnerability and pruning of phasic motoneuron axons in motoneuron disease alleviated by CNTF. Nat Neurosci 9:408–419.

Quinlan KA, Kajtaz E, Ciolino JD, Imhoff-Manuel RD, Tresch MC, Heckman CJ, Tysseling VM (2017) Chronic electromyograms in treadmill running SOD1 mice reveal early changes in muscle activation. J Physiol 595:5387–5400.

Quinlan KA, Lamano JB, Samuels J, Heckman CJ (2015) Comparison of dendritic calcium transients in juvenile wild type and SOD1G93A mouse lumbar motoneurons. Front Cell Neurosci 9:1–13 Available at: http://journal.frontiersin.org/article/10.3389/fncel.2015.00139/abstract.

Quinlan KA, Schuster JE, Fu R, Siddique T, Heckman CJ (2011) Altered postnatal maturation of electrical properties in spinal motoneurons in a mouse model of amyotrophic lateral sclerosis. J Physiol 589:2245–2260 Available at: http://doi.wiley.com/10.1113/jphysiol.2010.200659.

Raynor EM, Shefner JM (1994) Recurrent inhibition is decreased in patients with amyotrophic lateral sclerosis. Neurology 44:2148–2153.

Restrepo CE, Lundfald L, Szabó G, Erdélyi F, Zeilhofer HU, Glover JC, Kiehn O (2009) Transmitter-phenotypes of commissural interneurons in the lumbar spinal cord of newborn mice. J Comp Neurol 517:177–192.

Rothstein JD, Martin LJ, Kuncl RW (1992) Decreased Glutamate Transport by the Brain and Spinal Cord in Amyotrophic Lateral Sclerosis. N Engl J Med 326:1464–1468.

Saba L, Viscomi MT, Caioli S, Pignataro A, Bisicchia E, Pieri M, Molinari M, Ammassari-Teule M, Zona C (2016) Altered Functionality, Morphology, and Vesicular Glutamate Transporter Expression of Cortical Motor Neurons from a Presymptomatic Mouse Model of Amyotrophic Lateral Sclerosis. Cereb Cortex 26:1512–1528.

Saba L, Viscomi MT, Martini A, Caioli S, Mercuri NB, Guatteo E, Zona C (2019) Modified age-dependent expression of NaV1.6 in an ALS model correlates with motor cortex excitability alterations. Neurobiol Dis 130:104532 Available at: https://doi.org/10.1016/j.nbd.2019.104532.

Sangari S, Iglesias C, El Mendili MM, Benali H, Pradat PF, Marchand-Pauvert V (2016) Impairment of sensory-motor integration at spinal level in amyotrophic lateral sclerosis. Clin Neurophysiol 127:1968–1977.

Saxena S, Roselli F, Singh K, Leptien K, Julien JP, Gros-Louis F, Caroni P (2013) Neuroprotection through Excitability and mTOR Required in ALS Motoneurons to Delay Disease and Extend Survival. Neuron 80:80–96 Available at: http://dx.doi.org/10.1016/j.neuron.2013.07.027.

Shefner JM, Logigian EL (1998) The mixed nerve silent period in normal subjects and patients with amyotrophic lateral sclerosis. Electromyogr Clin Neurophysiol 38:505–510.

Siembab VC, Smith CA, Zagoraiou L, Berrocal MC, Mentis GZ, Alvarez FJ (2010) Target selection of proprioceptive and motor axon synapses on neonatal V1-derived Ia inhibitory interneurons and Renshaw cells. J Comp Neurol 518:4675–4701.

Vinsant S, Mansfield C, Jimenez-Moreno R, Moore VDG, Yoshikawa M, Hampton TG, Prevette D, Caress

J, Oppenheim RW, Milligan C (2013) Characterization of early pathogenesis in the SOD1G93A mouse model of ALS: Part II, results and discussion. Brain Behav 3:431–457.

Wainger BJ, Kiskinis E, Mellin C, Wiskow O, Han SSW, Sandoe J, Perez NP, Williams LA, Lee S, Boulting G, Berry JD, Brown RH, Cudkowicz ME, Bean BP, Eggan K, Woolf CJ (2014) Intrinsic membrane hyperexcitability of amyotrophic lateral sclerosis patient-derived motor neurons. Cell Rep 7:1–11 Available at: http://dx.doi.org/10.1016/j.celrep.2014.03.019.

Whitehouse PJ, Wamsley JK, Zarbin MA, Price DL, Tourtellotte WW, Kuhar MJ (1983) Amyotrophic lateral sclerosis: Alterations in neurotransmitter receptors. Ann Neurol 14:8–16.

Willis W, Willis JC (1964) Location of Renshaw Cells. Nature 204:1214–1215.

Wootz H, Fitzsimons-Kantamneni E, Larhammar M, Rotterman TM, Enjin A, Patra K, André E, Van Zundert B, Kullander K, Alvarez FJ (2013) Alterations in the motor neuron-renshaw cell circuit in the Sod1G93Amouse model. J Comp Neurol 521:1449–1469.

Zeilhofer HU, Studler B, Arabadzisz D, Schweizer C, Ahmadi S, Layh B, Bösl MR, Fritschy JM (2005) Glycinergic neurons expressing enhanced green fluorescent protein in bacterial artificial chromosome transgenic mice. J Comp Neurol 482:123–141.